[paper submitted to Journal of European Ceramic Society under the scope of JECS Trust contract number 2018193 – REVISION 1 - November 2019]

Modelling the particle contact influence on the Joule heating and temperature distribution during FLASH sintering

Ricardo Serrazina[1], Paula M. Vilarinho[1*], Ana M. O. R. Senos[1], Luis Pereira[2], Ian M. Reaney[3], Julian S. Dean[3*]

[1] Department of Materials and Ceramic Engineering, CICECO – Aveiro Materials Institute, University of Aveiro, 3810-193 Campus Santiago, Portugal
[2] CENIMAT-I3N, School of Science and Technoloy, FCT-NOVA, Universidade NOVA de Lisboa, Campus da Caparica. 2829-516 Caparica, Portugal
[3] Materials Science and Engineering, University of Sheffield, Sheffield S1 3JD, UK.

*Corresponding authors: paula.vilarinho@ua.pt, j.dean@shef.ac.uk

Abstract

FLASH sintering is a field-assisted technique that allows the densification of ceramics in a few seconds at temperatures significantly lower than those of conventional cycles. There is still discussion among the scientific community about the mechanism behind this sintering process, that has been typically attributed to Joule heating, defect creation and movement or liquid phase assisted sintering. Computational modelling can be a powerful tool in helping to explain and predict this process. Using potassium sodium niobate (KNN) as a case study, a lead-free piezoelectric, this work explores Finite Element Modelling to evaluate the dependence of Joule heating generation and temperature distribution as a function of the cubic particle orientation.

Introduction

Sintering is a well-established technique to consolidate powders using high temperatures. Among all know techniques, FLASH sintering provides rapid densification of particulate materials through the combination of external and Joule heating, the latter generated by relatively low current densities, *J*, as result of an applied electric field (*E*) directly within the specimen. This process does not require pressure, specific atmospheres or specialised dies. Thus, FLASH sintering has the potential to be a cost-effective, energy-efficient technique for densifying ceramics [1]. FLASH sintering was first reported for graphite powders by Lewis *et al.* [2] and more recently exploited by M. Cologna and co-workers to sinter oxides, such as yttria-stabilized zirconia, YSZ. Densification in less than 60s was reported with a temperature reduction of ~ 600 ºC, compared with conventional sintering [3]. The FLASH technique has been used to densify a wide variety of materials with YSZ one of the most studied systems. Simple oxides and carbides, such as alumina, zirconia, titania or silicon carbide have also been studied with further published work on ternary compounds such as strontium titanate or niobate systems [4]–[8].

When FLASH occurs, the material undergoes changes observable through two events; the so-called FLASH signatures that consist of a sudden shrinkage and a non-linear increase in conductivity. This is followed by an increase in the power dissipated by the system under current limit [9]. Without this current limit, the specimen would draw too much current and melt instead of densifying. This allows an abrupt shrinkage at furnace temperatures significantly lower than those of conventional sintering. Typically, the sintering temperature is decreased as the magnitude of the applied field increases [10].

During a constant heating rate FLASH experiment, three distinct stages can be identified: stage I, incubation, in which an electric field is applied, with no significant current draw; stage II, FLASH event, when the current drawn increases non-linearly with the furnace temperature and a spike in dissipated power is registered; stage III, steady state, where current is limited and held constant while the material undergoes the remaining shrinkage towards full densification [10], [11]. Such an out-of-equilibrium phenomenon is complex, but two main theories have been proposed [4], [9], [10]. Thermal runaway through Joule heating is one of the widest accepted theories. In this proposed mechanism, the rate of

generated Joule heat is higher than heat dissipation, inducing a very fast increase in temperature during stages II and III of FLASH and therefore responsible for the abrupt densification [12]–[15]. Liquid phase formation and viscous flow has also been associated to Joule heating effects. The formation of a liquid phase upon grain boundaries and small particle melting suggests the existence of thermal gradients between particle surfaces and cores [16]–[19].

Despite good agreement with the onset criterion for FLASH, thermal runaway does not explain the increase in specimen conductivity nor the light emission from the materials upon FLASH [10]. Defect generation and movement induced by the relatively high electric fields have been shown to have a high influence in FLASH sintering, namely in semi-conductors and ionic conductors [20]–[23]. However, work by Biesuz and Sglavo [10] and Cologna *et al.* [24] concluded that the neck growth rate of 3YSZ is unaffected when the samples are subject to electric fields similar to those used in FLASH, i.e. the electric field by itself has no influence on particle welding and surface diffusion. In accordance with Biesuz, FLASH should be considered as a current- rather than field- (voltage) assisted sintering process [10].

Several mathematical models have been shown to explain a specific stage or phenomena of FLASH. For example, the thermal runaway model for describing the onset condition for the uncontrolled heating process, triggering FLASH sintering, was independently developed by Todd *et al.* [14] and Zhang *et al.* [15] in 2015. Furthermore, the black body radiation model has been largely used to estimate specimen temperature. Grasso *et al.* [25] have shown through the use of computational modelling, that the macroscopic temperature distribution in a YSZ dog-bone shape is uniform within the gauge section but heterogeneous in the electrode contacting areas. In contrast with Grasso's work, M. Yoshida and co-workers found that dog-bone-like specimens present an non-homogeneous macroscopic distribution of current density, power dissipation and temperature during stage III of FLASH [26].

Our previous work using Finite Element Modelling (FEM) to map out the Joule heating distribution in cubic particles upon FLASH has shown that the heat generation magnitude is dependent on the contact area and geometry. As the contact area becomes smaller, the Joule heating is higher and more localized.

Such observations suggested that a temperature non-uniformity between particle surface (contacts) and core is created [27].

Potassium sodium niobate, ($K_{0.5}Na_{0.5}NbO_3$, KNN) is a lead-free piezoelectric potentially suggested as a replacement for the market-leader, lead zirconate titanate in piezoelectric applications [28], [29]. KNN possesses a cuboid particle shape, that influences its densification; important in FLASH since surface phenomena are critical [30]. KNN was previously FLASH sintered at 900 ºC to 94 % of its theoretical density and it was shown that the densification mechanism was related to the formation of core-shell structures with non-homogeneous distribution of alkali Na and K [7].

However, no studies on the local Joule heating effect, nor thermal gradient were presented. Until now, the local temperature distribution as a function of Joule heating during FLASH sintering has not been studied. Furthermore, the modelling of FLASH process through the three stages has not been presented. In this work, we used *COMSOL Multiphysics* [31] to set up a time dependent modeling procedure to simulate the evolution of the FLASH process in a given microstructure.

Experimental

Powder production and processing

KNN powders were produced by a conventional solid-state route as previously reported [32]. Ultra-high purity alkali carbonates and niobium oxide (99.99 %) were used, and the precursors ball milled in ethanol. Calcination was performed at 900 ºC for 3 h. KNN was ball milled 24 h after calcination, and uniaxially and isostatically pressed (130 and 250 MPa, respectively) into ca. 15 x 5 x 2 mm pellets.

Pellets were FLASH sintered, and the DC electrical conductivity measured throughout the process to provide experimental inputs for the finite element model. The conductivity of green pellets (relative density, ρ = 65 $\pm$ 3 %) was measured using an alumina sample holder and platinum contact sheet electrodes, at a constant heating rate of 10 K/min, with an electric field of 300 V/cm and current limited to 20 mA/mm^2. Densities > 90 % were obtained after FLASH sintering for 60 s. Specimen displacement, current and voltage were

recorded during FLASH experiments, and the respective relative length variation, conductivity and power dissipation were calculated and are shown, as a function of the measured temperature, in

Figure 1 a). The temperature was measured with a thermocouple, placed within a distance of 5 to 7 mm from the specimen. Figure 1 b) shows a magnification of a), overlaid with the fitted conductivity. The three distinct FLASH stages are identified, consistent with previous work [10].

a)

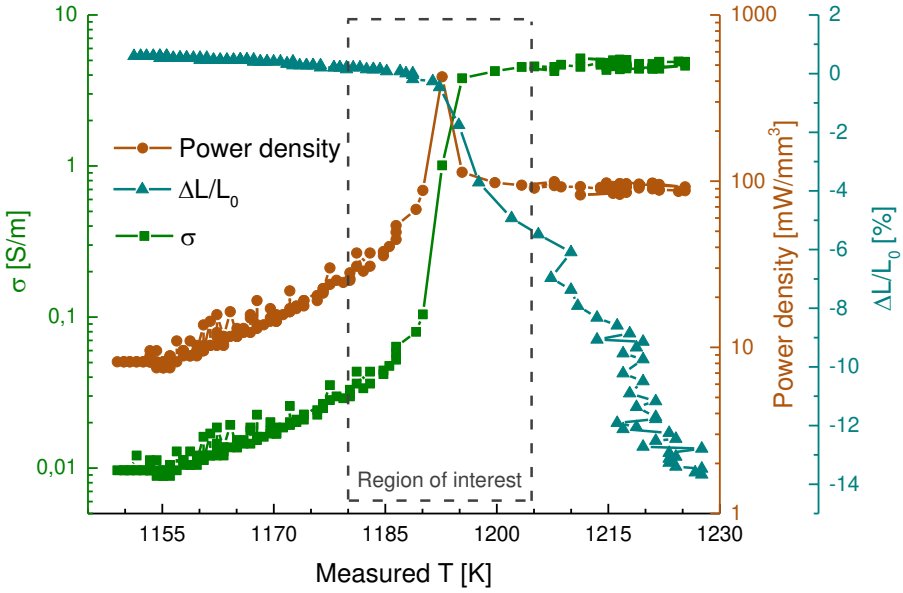

b)

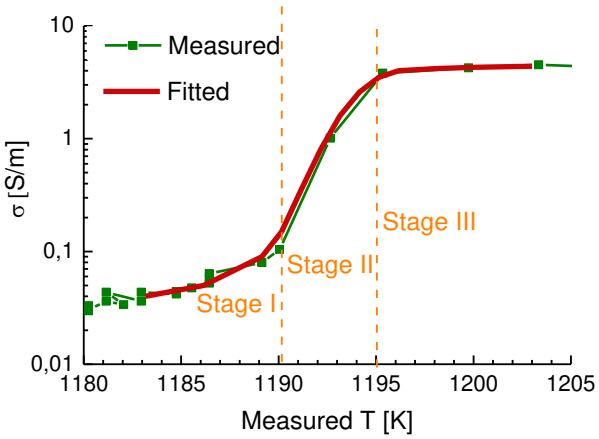

Figure 1 – (a) Measured relative displacement (light blue, ▲), conductivity (green, ■) and power dissipation (brown, ●) dependence with measured temperature, for KNN under 300 V/cm and 20 mA/mm^2 current limit; the experimental time interval between each acquired point is 1 s. (b) magnification of a), with measured (green) and fitted (red) conductivity dependence with measured temperature; the three stages of FLASH are identified and separated by orange dashed lines.

Figure 2 shows the microstructure of a green KNN specimen heated at 900 ºC (1173,15 K) for 30 min, with no electric field applied. The cuboid particle shape, characteristic of KNN, induces anisotropy in the contact between particles. This provides a qualitative structure of packed cuboid grains that will be replicated in the FEM model. To simplify the model, the cuboid particles were considered to contact through flat surfaces, edges or vertexes. Also, as shown in Figure 2, the particle size of pre-FLASH ceramic is typically < 3 μm; most particles are micron-sized, with a few small particles, 0.2 to 0.5 μm.

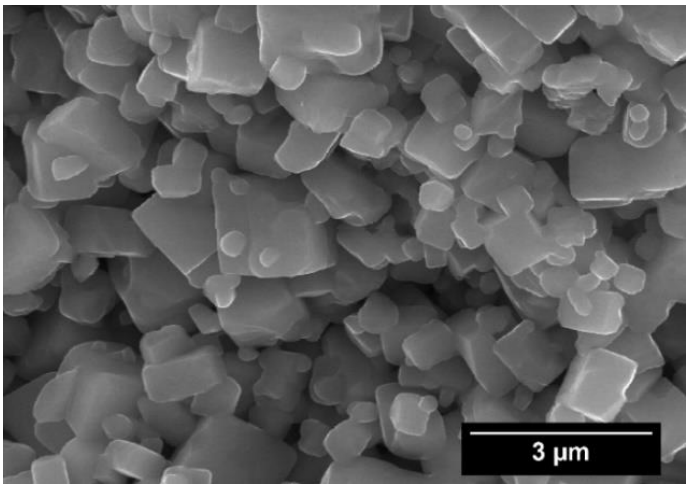

Figure 2 – SEM micrograph of green KNN body, heated at 1173 K for 30 min, showing the pre-FLASH microstructure that is implemented in the model.

Modelling

The local Joule heating and temperature distribution within the particle as a function of time were simulated in *COMSOL Multiphysics* models [31]. This

included a thermal dependence change in the conductivity of KNN during the FLASH sintering process.

To mimic the experimental process and observe the effect of the microstructure, a range of different particle orientation were generated. A potential difference of $9x10^{-5}$ V (in the case of face contacts) was applied across the longitudinal surfaces of the system (Figure 3 shows the schematic representation of DC voltage application). This voltage was calculated for each particle arrangement by scaling the 300 V/cm applied field.

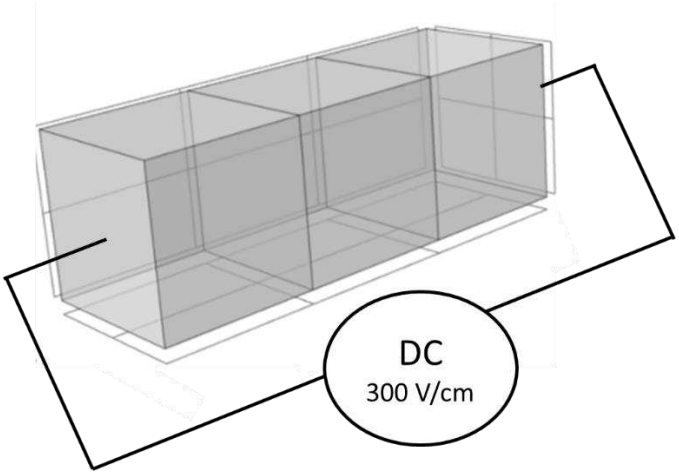

Figure 3 – Representation of DC voltage application onto particle arrangements. Example for face contacting cuboids.

During stage I and stage II, where no current limit is imposed, the current density in the sample constantly increases as result of the increase in the electrical conductivity with temperature. In stage III the voltage rises until the current density reaches the nominal 20 mA/mm^2. At this point, the model becomes current controlled. Such control allows the model to accurately represent the three stages of FLASH as a function of the experimentally measured temperature.

To describe the electric field and current control during the 3 stages of FLASH sintering by FEM, the electric potential was applied to the different arrangement of particles through the use of a *terminal* function. The end faces (Figure 3) were assigned to be either *terminal* or *ground*, while all the other surfaces were assigned with *electric insulation*. The *terminal* was associated with g*lobal equation* functions, responsible during stage I and II in limiting and

recording the current. This allows the model to maintain a 300 V/cm electric field. During stage III, the *terminal is set to* control the current to the pre-set value of 20 mA/mm^2, limiting the applied potential.

After stage II, a relevant shrinkage starts to occur on the specimen (Figure 1). To reflect this observation, COMSOL models were assigned a linear shrinkage of 4 %. For simplification, the shrinkage was considered to occur only at the middle particle. For edge and vertex contact cases, a respective increase of contact area was considered.

A *Thermal insulation* boundary condition was considered to all the faces, with no further radiation nor convection heat transfer concern. Such approximation should not compromise the validity of the simulations, as this meso-scale model is intended to simulate only the Joule heating and local temperature distribution in μm-sized particles. For the description of the complete FLASH curve (

Figure 1), the fitted conductivity curve was integrated into small temperature steps, typically of 1 K. The starting temperature was 913 ºC (1186.15 K) and the particles assigned to the KNN properties (σ = 0.05 S/m,

Figure 1) for that specific condition. The model was run and halted when the next integrated temperature was reached (in this case, when T = 1187.15 K). The Joule heating and temperature distributions were recorded, and the particles electrical conductivity updated for the next temperature to be considered. This was then repeated to describe all experimental points in the conductivity curve. Two outputs are used to study the FLASH process: (i) the total power dissipation density, considered as Joule heating, and temperature distribution at the end of each integration step; (ii) the modelled time interval between each integration step. For each integration step, the reference temperature in the model was updated. A representation of the integration steps for stage II is shown in Figure 4.

Due to the speed of the process, and to simplify the model, we assume that there is no heat dissipation from the particles to the surrounding environment. It is thus expected that the modelled integration time, i.e., the small integration steps, will be less than that measured experimentally, which is ca. 3 s between beginning and end of stage II, and ca. 10 - 15 s for the all interest region, from

1180 to 1205 K (Figure 1). Grain boundaries were not considered in this simple model. The properties of such structures, namely, their conductivity and size, are yet being studied and core-shell structures might describe more precisely the system. Furthermore, thermal conductivity and specific heat capacity of bulk KNN were considered constant and set as 2.6 W/(m.K) and 800 J/(kg.K), respectively.

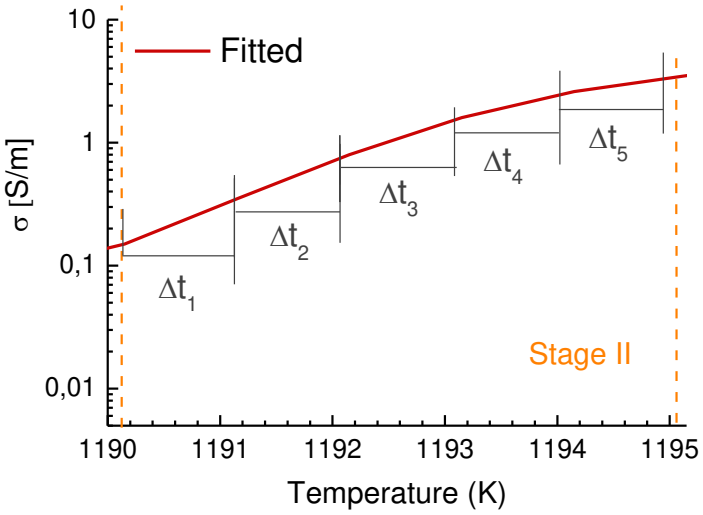

Figure 4 – Integration steps demonstration for stage II of FLASH. This is a magnification for the fitted conductivity curve of Figure 1 b) during stage II.

Results and discussion

Three cubic particles, of 1 μm length, were described in the model and placed in a series arrangement. The three possible orientations, resulting in face/face, face/edge and face/vertex type contacts are shown in Figure 5.

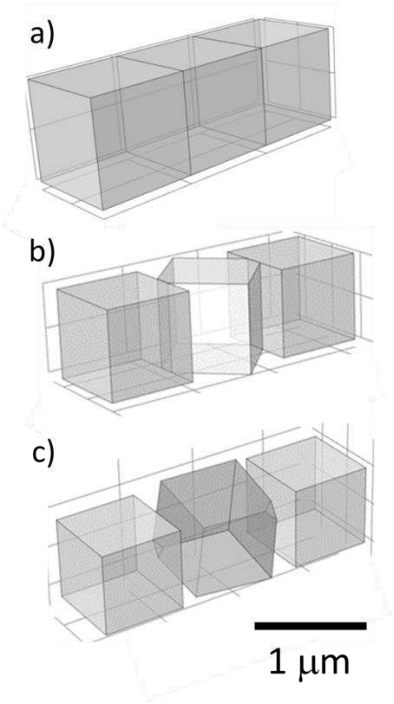

Figure 5 - Representation of “in-series” cubes contacting with (a) faces, (b) face/edge and (c) face/vertex, respectively from left to right.

Electric field, current density, and Joule heating (or total power dissipation density) were simulated using the process described above. The results for face/face contacts are shown in supplementary information (SI) figure 1**Error! Reference source not found.** (a), (b) and (c), respectively. The three stages of FLASH, the latter part of stage I, stage II and stage III are shown in vertical order. The respective conductivity vs. temperature dependence and the points being simulated are highlight in supplementary information (SI) figure 1 d). Results show good agreement with experimental conditions (electric field of 300 V/cm and current limit of 20 mA/mm^2). During stage II, the current density is slightly increased over the limit placed on the value. This is agrees well with experimentally data obtained (Figure 1 (a)) and published [9], [10], that shows a power spike upon FLASH onset during stage II. Such particle configuration should not generate disorder or anisotropy in the electric field generation and current flow, due to the lack of geometry disorder (as sharp contact or edges, for instance); thus, it is suitable for validating this approach.

As shown in the supplementary information (SI) figure 1, for models where the three particles are in face/face contact, a uniform distribution of Joule heating is generated. With no discontinuities in either shape or properties, or grain

boundaries present, the system behaves as one single block. The maximum dissipated power can be seen to be generated during stage II, in accordance with the maximum current density.

Joule heating distributions for face/edge and face/vertex particle configuration for the three stages of FLASH are shown in Figure 6 (a) and (b), respectively and behave differently. Figure 6 (c) highlights the corresponding FLASH stages, with the conductivity fitted curve overlaid with grey circles. For the edge contact (Figure 6 (a)), non-uniform Joule heating distributions were generated, directly related to the contact area. In the sharp contact edge, Joule heating is, typically, three orders of magnitude higher than in the "far-from-contact" areas. Further increase was determined as the contact area decreases, as is the case of the face/vertex configuration (Figure 6 (b)). Furthermore, cross-sectional plane views are represented for late stage I for both edge and vertex geometry and show that Joule heating distribution on the surface of the particles is similar to that of grain cores, revealing again the Joule heating concentration on the particle-particle contact areas.

Overall electric power simulations of stage III, shown in SI figure 2, for both geometries do not show any gradients. The total power is found to be between 0.9 – $2x10^{-18}$ W and not concentrated on the particle contacts, because this is a volume independent variable. These simulated power values may seem low, however for a net power of $1x10^{-18}$ on a volume of 1 μm^3 would result in a power density of 1 W/m^3 (or $1x10^{-6}$ mW/mm^3), which relates well with the low Joule heating dissipation areas on the previously discussed Figure 6 a) and b). The overall particle surfaces (except the contacting ones) of face and vertex contacts presented, respectively, a light red and light orange color in Joule heating representations. These colors represent a power dissipation (or Joule heating) of ca. 100 mW/mm^3 which relates very well with experimental observations (Figure 1 a)).

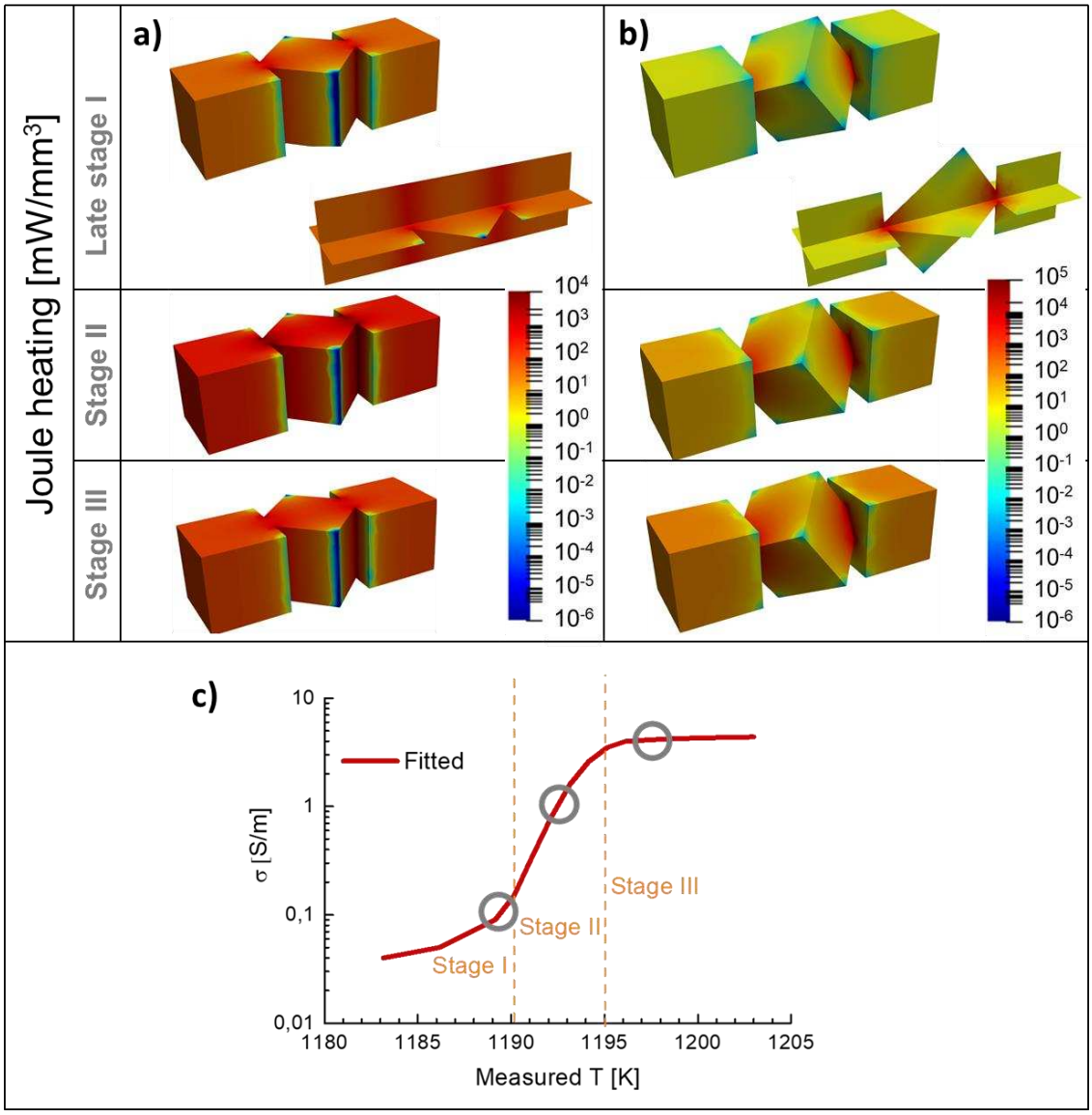

Figure 6 – Joule heating distribution (in mW/mm^3) for sharp contact arrange of particles: (a) face/edge and (b) face/vertex. Three snapshots of the FLASH process are shown, corresponding to late stage I, stage II and stage III. A section view for late stage I case is also shown, for clarification. (c) represents the corresponding stages with the conductivity fitted curve overlaid with grey circles.

The proposed model suggests that the maximum Joule heating increases two orders of magnitude from face/face contact compared to face/vertex. As the contact area is decreased and made sharper, the Joule heating intensity increases due to the increased local current density. Interestingly, the higher

values of Joule heating are typically observed for stage II of FLASH, specifically in face/face case, in which no contact shape influence is expected. Such observation explains the experimentally measured fast increase in temperature during stage II of FLASH sintering.

The temperature distribution for cubes with face/edge (a) and face/vertex (b) contacts for late stage I in the simulated FLASH process can be seen in SI Figure 3 and do not show any thermal gradients, with similar results for stage II and II.

Following the work presented by W. Ji and co-workers [33], thermal diffusivity of KNN, α, was calculated under the conditions of our model: α = 7.2×10^{-7} m^2/s. The respective time for thermal equilibrium is defined as D^2/α, where D is the distance. For D = 1 μm (micron-sized particles), equilibrium time is equal to 1.4×10^{-6} s. Such micro-scale time for temperature equilibrium did not allow to observe any thermal gradient on the integration approximation of our simulations. On the other hand, when simulation integration time is changed to 0.5 μs (graphical results not shown), thermal gradients were only observable on the 5^{th} decimal place of temperature scale.

This suggests that when 1 µm side cubes (1x1x1 µm) KNN particles are considered in the defined conditions, there are no significant thermal gradients between grains, since they are suppressed by the heat dissipation from surface to core. The lack of radiation and thermal dissipation from the particles towards the environment may contribute to the unexpected homogeneous temperature distribution, because diffusive effects would decrease particle surface temperature and increase the temperature difference between the heat source (particle contacts) and surfaces. On the other hand, the exclusion of grain boundaries from the model or defect formation and movement contributions may also explain the absence of observable temperature gradients between particle contact zones and the core.

Despite the lack of thermal gradients observation on the simulated scenarios, liquid phase formation on grain boundaries of FLASH sintering ceramics has been observed [18], [27], [34], [35]. A plausible explanation for such observations is that the fast heating upon grain boundaries allows the formation of low melting point phases that contribute for grain boundary amorphization and particle sliding, as previously proposed [27].

Despite the recognize limitation of the model, the suggested absence of temperature gradients might also be directly related with the speed of heat dissipation from contacts to particle cores. The simulated time of each integration step was determined by the model. In each condition, the theoretical/simulated time between integration step *n* and *n+1* was determined. The simulations were run for each particle contact scenario and results of cumulative time evolution are represented in Figure 7. Each point of the curve represents an integration step. Note that the total FLASH time between the beginning of stage I and beginning of stage III (region of interest in Figure 1 (a)) was measured experimentally to be 10 to 15 s.

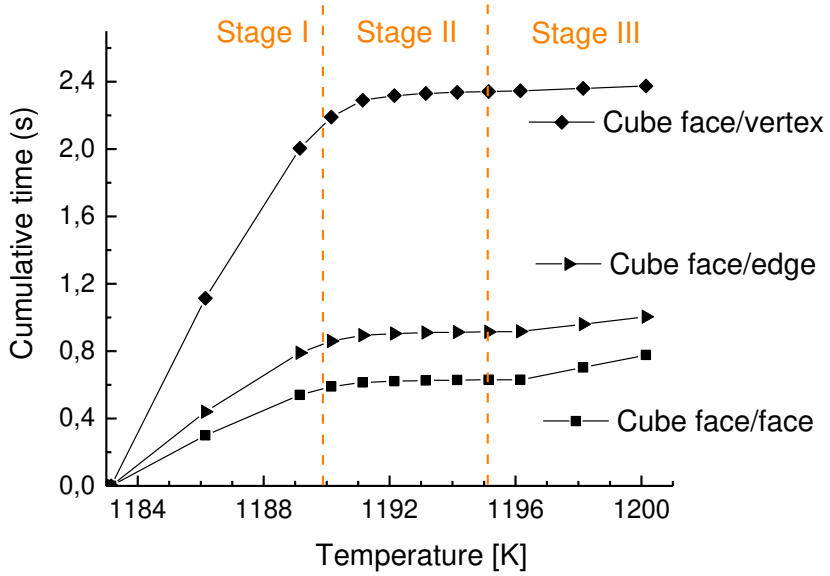

Figure 7 – Cumulative time needed to reach the correspondent temperature for cubes with face contacts (squares) face/edge (triangles) and face/vertex (diamond).

From Figure 7 we conclude that:

(i) Regardless of the particle contact area and type, the time extracted from the model is lower than that observed experimentally during FLASH process, potentially because heat dissipation by the specimen is not considered in the model. However, the simulated times are comparable.

(ii) For stage I, the sharper the contact area, the slower the heating process by Joule heating. Despite the higher recorded local current density for sharper contacts (Figure 6), the Joule heating requires more time to dissipate through the particles (not to the environment). This observation can further explain non-uniformity in specimen densification by FLASH sintering [36].

(iii) During stage II, the time evolution behaviour is independent of the contact type. There is a significant increase in temperature, as the cumulative time dependence has an almost zero gradient. This is consistent with experimental observations during stage II of FLASH process.

(iv) For stage III, the vertex configuration maintains an almost zero gradient. As such, we find configurations with blunter contacts (e.g. edge or faces as opposed to vertexes) heat up more slowly due to current limiting conditions in this stage.

The proposed model and observations suggest that the process can be summarised as the following:

(i) At stage I there is a homogeneous heat generation which spreads from the contact region to the surrounding particles.

(ii) During stage II, the high thermal gradients and localized heat in the contact region explain the non-linear behaviour of specimen temperature, conductivity and significant thermal runaway that are typical of stage II.

(iii) Despite the significant non-uniform Joule heating generation, we find that, in the conditions of this model, micron-sized particles dissipate all the generated heat at a higher rate than that necessary to register relevant thermal gradients.

Although negligible thermal gradients are observed, we note that this model does not account for grain boundary behaviour nor defect movement nor even thermal dissipation through the environment. In these conditions, the proposed simulations allow the conclusion that thermal gradients from Joule heating generation should not be observed during FLASH sintering.

However, previously reported observations and theoretical descriptions of amorphized grain boundaries in FLASH sintered ceramics and liquid phase formation during FLASH [18], [27], [34], [35] suggest, at least, two possibilities: (i) significant thermal gradients are formed during FLASH sintering and/or (ii) compositional changes arising from current flow promote low melting point phase formation and their preferential melting without significant temperature gradients between particles and grain boundaries. The proposed model aimed to depict the first hypothesis; however, results show that, in the conditions of the simulations, micron-sized particles dissipate the possible heat gradients at a rate, too fast to identify in this model.

Further modelling work is now being developed to describe grain boundaries as shells covering the bulk core of ceramics, and their influence on temperature gradients. Moreover, low melting point phases are being considered at the grain boundaries.

Conclusion

In this work we show that the proposed Finite Element Model describe FLASH sintering experiments with particle orientation dependences. Despite the significant Joule heating and non-uniform distribution found for sharp edges contacts, no relevant thermal gradients between particle surfaces and cores are found. We conclude that if differences in grain boundary electrical conduction in respect to the bulk and heat dissipation to the surrounding environment are neglected, Joule heating alone does not contribute to temperature gradients in micron-sized particles, even when very sharp contacts are considered. However, one important output of this model is that grain boundaries are mandatory to account for liquid phase formation at particle contacts during FLASH sintering. Further works should include the grain boundary description using, as for instance, core-shell structures. Moreover, models are now being developed to account for heat dissipation and radiation through the environment. Nevertheless, it was shown that simple modelling techniques as FEM can be useful to understand and depict the FLASH phenomena, isolating contributions of different events in the process.

Acknowledgements

The authors are grateful to the JECS Trust for funding the visit of Ricardo Serrazina to University of Sheffield (Contract No. 2018193). This work was also developed within the scope of the project CICECO-Aveiro Institute of Materials, FCT Ref. UID/CTM/50011/2019, financed by national funds through the FCT/MCTES. This work was also financed by Portugal 2020 through European Regional Development Fund (ERDF), in the frame of Operational Competitiveness and Internationalization Programme (POCI), in the scope of the project "FLASH sintering of lead free functional oxides towards sustainable processing of materials for energy and related applications - FLASH", POCI-01-0247-FEDER-029078. Ricardo Serrazina acknowledges FCT for financial support (SFRH/PD/BD/128411/2017).

References

[1] J. Luo, "The scientific questions and technological opportunities of flash sintering: From a case study of ZnO to other ceramics," *Scr. Mater.*, vol. 146, pp. 260–266, 2018.

[2] F. A. Lewis, J. Orr, and A. R. Ubbelohde, "Contact Effects resulting from Compression and Flash Sintering in Graphite Powders," *Proc. Phys. Soc. Sect. B*, vol. 70, no. 10, pp. 928–936, Oct. 1957.

[3] M. Cologna, B. Rashkova, and R. Raj, "Flash Sintering of Nanograin Zirconia in <5 s at 850°C," *J. Am. Ceram. Soc.*, vol. 93, no. 11, pp. 3556–3559, Nov. 2010.

[4] M. Yu, S. Grasso, R. Mckinnon, T. Saunders, and M. J. M. Reece, "Review of flash sintering: materials, mechanisms and modelling," *Adv. Appl. Ceram.*, vol. 116, no. 1, pp. 1–37, 2017.

[5] L. A. Perez-Maqueda, E. Gil-Gonzalez, A. Perejon, J. M. Lebrun, P. E. Sanchez-Jimenez, and R. Raj, "Flash sintering of highly insulating nanostructured phase-pure $BiFeO_3$," *J. Am. Ceram. Soc.*, vol. 100, no. 8, pp. 3365–3369, 2017.

[6] N. Shomrat, S. Baltianski, C. A. Randall, and Y. Tsur, "Flash sintering of potassium-niobate," *J. Eur. Ceram. Soc.*, vol. 35, no. 7, pp. 2209–2213, 2014.

[7] G. Corapcioglu, M. A. Gulgun, K. Kisslinger, S. Sturm, S. K. Jha, and R.

Raj, “Microstructure and microchemistry of flash sintered $K_{0.5}Na_{0.5}NbO_3$,” *J. Ceram. Soc. Japan*, vol. 124, no. 4, pp. 321–328, 2016.

[8] F. Lemke, W. Rheinheimer, and M. J. Hoffmann, “A comparison of power controlled flash sintering and conventional sintering of strontium titanate,” *Scr. Mater.*, vol. 130, pp. 187–190, 2017.

[9] C. E. J. Dancer, “Flash sintering of ceramic materials,” *Mater. Res. Express*, vol. 3, no. 10, pp. 102001–102025, 2016.

[10] M. Biesuz and V. M. Sglavo, “Flash sintering of ceramics,” *J. Eur. Ceram. Soc.*, vol. 39, no. 2–3, pp. 115–143, 2019.

[11] S. K. Jha, K. Terauds, J. Lebrun, and R. Raj, “Beyond flash sintering in 3 mol % yttria stabilized zirconia,” *J. Ceram. Soc. Japan*, vol. 124, no. 4, pp. 283–288, 2016.

[12] Y. Dong and I. W. Chen, “Onset Criterion for Flash Sintering,” *J. Am. Ceram. Soc.*, vol. 98, no. 12, pp. 3624–3627, 2015.

[13] R. Raj, “Joule heating during flash-sintering,” *J. Eur. Ceram. Soc.*, vol. 32, no. 10, pp. 2293–2301, 2012.

[14] R. I. Todd, E. Zapata-Solvas, R. S. Bonilla, T. Sneddon, and P. R. Wilshaw, “Electrical characteristics of flash sintering: Thermal runaway of Joule heating,” *J. Eur. Ceram. Soc.*, vol. 35, no. 6, pp. 1865–1877, 2015.

[15] Y. Zhang, J. Il Jung, and J. Luo, “Thermal runaway, flash sintering and asymmetrical microstructural development of ZnO and ZnO-Bi_2O_3 under direct currents,” *Acta Mater.*, vol. 94, pp. 87–100, 2015.

[16] R. Chaim and C. Estournès, “On thermal runaway and local endothermic/exothermic reactions during flash sintering of ceramic nanoparticles,” *J. Mater. Sci.*, pp. 1–12, 2018.

[17] R. Chaim and C. Estournès, “Effects of the fundamental oxide properties on the electric field-flash temperature during flash sintering,” *Scr. Mater.*, vol. 163, pp. 130–132, 2019.

[18] R. Chaim, “On the kinetics of liquid-assisted densification during flash sintering of ceramic nanoparticles,” *Scr. Mater.*, vol. 158, pp. 88–90, 2019.

[19] R. Chaim, “Liquid film capillary mechanism for densification of ceramic powders during flash sintering,” *Materials (Basel).*, vol. 9, no. 4, pp. 19–21, 2016.

[20] A. R. Genreith-Schriever and R. A. De Souza, “Field-enhanced ion

transport in solids: Reexamination with molecular dynamics simulations," *Phys. Rev. B*, vol. 94, no. 22, p. 224304, Dec. 2016.

[21] M. Schie, S. Menzel, J. Robertson, R. Waser, and R. A. De Souza, "Field-enhanced route to generating anti-Frenkel pairs in HfO_2," *Phys. Rev. Mater.*, vol. 2, no. 3, p. 035002, Mar. 2018.

[22] S. K. R. S. Sankaranarayanan, E. Kaxiras, and S. Ramanathan, "Electric field tuning of oxygen stoichiometry at oxide surfaces: molecular dynamics simulations studies of zirconia," *Energy Environ. Sci.*, vol. 2, no. 11, p. 1196, Nov. 2009.

[23] M. Jongmanns, R. Raj, and D. E. Wolf, "Generation of Frenkel defects above the Debye temperature by proliferation of phonons near the Brillouin zone edge," *New J. Phys.*, vol. 20, no. 9, 2018.

[24] M. Cologna and R. Raj, "Surface diffusion-controlled neck growth kinetics in early stage sintering of zirconia, with and without applied DC electrical field," *J. Am. Ceram. Soc.*, vol. 94, no. 2, pp. 391–395, 2011.

[25] S. Grasso *et al.*, "Modeling of the temperature distribution of flash sintered zirconia," *J. Ceram. Soc. Japan*, vol. 119, no. 1386, pp. 144–146, 2011.

[26] M. Yoshida, S. Falco, and R. I. Todd, "Measurement and modelling of electrical resistivity by four-terminal method during flash sintering of 3YSZ," *J. Ceram. Soc. Japan*, vol. 126, no. 7, pp. 579–590, 2018.

[27] R. Serrazina, J. S. Dean, I. M. Reaney, L. Pereira, P. M. Vilarinho, and A. M. O. R. Senos, "Mechanism of densification in low-temperature FLASH sintered lead free Potassium Sodium Niobate (KNN) piezoelectrics," *J. Mater. Chem. C*, 2019.

[28] C.-H. Hong *et al.*, "Lead-free piezoceramics and Where to move on?," *J Mater.*, vol. 2, pp. 1–24, 2016.

[29] X. Wang *et al.*, "Giant piezoelectricity in potassium-sodium niobate lead-free ceramics," *J. Am. Chem. Soc.*, vol. 136, no. 7, pp. 2905–2910, 2014.

[30] M. A. Rafiq, M. E. Costa, A. Tkach, and P. M. Vilarinho, "Impedance analysis and conduction mechanisms of lead free potassium sodium niobate (KNN) single crystals and polycrystals: A comparison study," *Cryst. Growth Des.*, vol. 15, no. 3, pp. 1289–1294, 2015.

[31] "COMSOL Multiphysics® Software - Understand, Predict, and Optimize." [Online]. Available: https://www.comsol.com/comsol-multiphysics.

[Accessed: 18-Jul-2019].

[32] M. A. Rafiq, A. Tkach, M. E. Costa, and P. M. Vilarinho, “Defects and charge transport in Mn-doped $K_{0.5}Na_{0.5}NbO_3$ ceramics,” *Phys. Chem. Chem. Phys.*, vol. 17, no. 37, pp. 24403–24411, 2015.

[33] W. Ji, B. Parker, S. Falco, J. Y. Zhang, Z. Y. Fu, and R. I. Todd, “Ultra-fast firing: Effect of heating rate on sintering of 3YSZ, with and without an electric field,” *J. Eur. Ceram. Soc.*, vol. 37, no. 6, pp. 2547–2551, 2017.

[34] J. Gonzalez-Julian and O. Guillon, “Effect of Electric Field/Current on Liquid Phase Sintering,” *J. Am. Ceram. Soc.*, vol. 98, no. 7, pp. 2018–2027, 2015.

[35] R. Chaim and Y. Amouyal, “Liquid-Film Assisted Mechanism of Reactive Flash Sintering in Oxide Systems,” *Materials (Basel).*, vol. 12, no. 1494, pp. 1–9, 2019.

[36] Y. Du, A. J. Stevenson, D. Vernat, M. Diaz, and D. Marinha, “Estimating Joule heating and ionic conductivity during flash sintering of 8YSZ,” *J. Eur. Ceram. Soc.*, vol. 36, no. 3, pp. 749–759, 2016.

Supplementary Information.

SI Figure 1 a-c shows the simulated FLASH process for face/face contacted models. The conductivity change as a function of temperature for each of the stages is shown in figure 1 (d) with the specific stages that have been simulated highlight on the curve. A uniform distribution of Joule heating is generated through the systems. With no discontinuities in either shape or properties, or grain boundaries present, the system behaves as one single block. The maximum dissipated power can be seen to be generated during stage II, in accordance with the maximum current density.

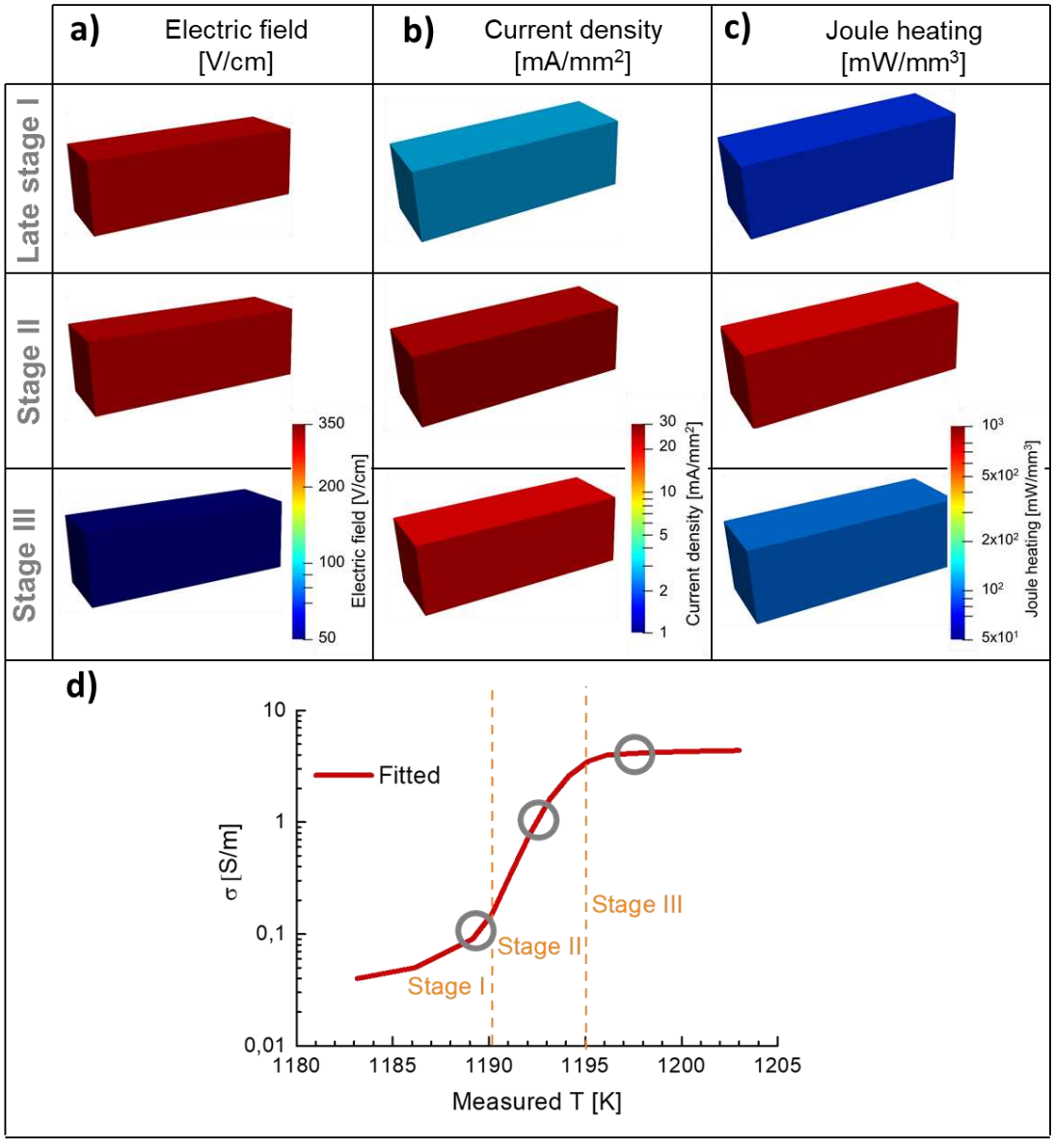

SI Figure 1 – Simulated electric field (a), current density (b) and total power dissipation density (or Joule heating) (c) for face/face contact particles. The respective conductivity over temperature curve is shown in (d) to highlight the simulated steps over the curve.

The electric power simulations of stage III are shown in SI figure 2, for both the face/edge and face/vertex models. While the total power is found to be between 0.9 – 2x10^{-18} W for the two geometries, no significant gradients are observed on the particle contacts

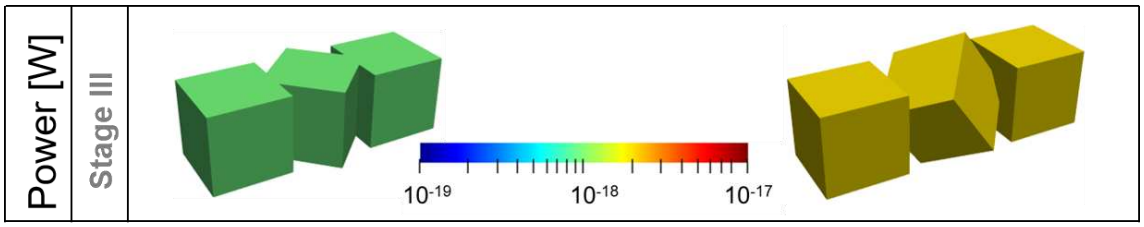

SI Figure 2 – a representation of total power for face/edge and face/vertex models. While the face/vertex shows higher power, no significant power gradients are observed.

Simulated temperature profiles are shown in SI figure 3. It should be noted that the temperature scale is the same for both representation and that similar representations of temperature distributions were found for stage II and III which are not shown here.

The temperature distribution for face/face contacts can be seen to be homogeneous, as expected, consistent with the results from SI figure 1. However, for sharp contacts, despite the tight scale used for temperature representation (a 0.80 K total variation) and contrary to expectation, the model does not show any thermal gradient for cubic particle contacts.

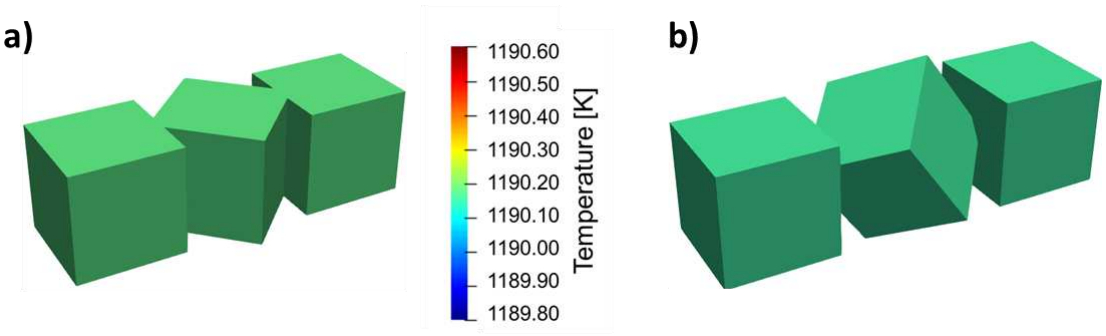

SI Figure 3 – Late stage I temperature representation (in K) for face/edge (a) and face/vertex (b) contacts. Temperature scale is the same for (a) and (b).